Engineering Failure Analysis 151 (2023) 107389

Contents lists available at ScienceDirect

Engineering Failure Analysis

journal homepage: www.elsevier.com/locate/engfailanal

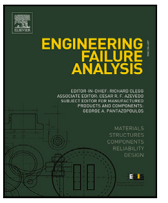

Dynamic response analysis of a model truss bridge considering damage scenarios

Patricia Vanova [a,b], Zhen Sun [c,d], Odin-Eliott Odinson [b], Zhiyu Jiang [b,*]

[a] Center of Research and Innovation in Construction, Faculty of Civil Engineering, Technical University of Kosice, Vysokoskolska 4, Kosice, 042 00, Slovakia

[b] Department of Engineering Sciences, Faculty of Engineering and Science, University of Agder, Jon Lilletuns vei 9, Grimstad, NO-4879, Norway

[c] Construct-ViBest, Faculty of Engineering (FEUP), University of Porto, R. Dr. Roberto Frias, Porto, 4200-465, Portugal

[d] Key Laboratory of Concrete and Prestressed Concrete Structures, Ministry of Education, Southeast University, Nanjing, 211189, China

ARTICLE INFO

Keywords:
Steel truss bridge
Random vibration
Fatigue cracks
Nodal acceleration
Finite element analysis

ABSTRACT

Structural health monitoring plays a key role for maintenance and lifetime extension of bridges under complex loading conditions and damage scenarios. This paper applies vibration-based methods to monitor the structural health of a Warren-type truss bridge. First, acceleration measurements are used to obtain natural frequencies and modal shapes of the bridge by modal identification. Then, a high-fidelity numerical model in a finite element code is calibrated. Damage scenarios with various crack location and severity are considered for a member, and time-domain simulations are carried out to assess the dynamic responses of the bridge under random excitation. An analysis of the acceleration statistics shows that the damaged member displays a more significant increase in accelerations than the intact members, and locations near the supports of the damaged member experience more changes than other locations. This study contributes to a fundamental understanding of bridge dynamics and facilitates development of damage identification methods.

1. Introduction

Railway or road steel truss bridges are subject to repeated dynamic loads during their lifetime. Such dynamic loads may arise from traffic actions or from ambient environments in the form of temperature, wind, and rain. According to the design standards of bridge structures, e.g., Eurocode [1], the traffic loads are typically considered using a dynamic amplification factor and the wind loads should be examined depending on the shape and length of the bridge. If not considered properly in the design, these loads could induce vibration of the bridge and eventually lead to premature failures.

For structural failures of steel bridges, several causes exist including fatigue [2], overload [3], corrosion [4], and collision [5]. Among them, fatigue is the most common cause of failure for steel truss bridges in the U.S. [5]. Fatigue cracks typically occur in the weakest locations that coincide in the joints between the individual members of a truss bridge [6–8], as depicted in Fig. 1. The development of cracks in steel profiles usually results in a reduction of the effective cross section, and afterwards in the overall reduction in the stiffness of a bridge. The fatigue cracks and subsequent changes in the structural properties of any bridges must be detected at an early stage. Otherwise, the lifespan of the bridges can be significantly shortened and there is a risk of collapse. In the past, collapses of several bridges were reported [9]. Such catastrophes can cause casualties, disruption in transportation and negative economic impacts.

* Corresponding author.
E-mail address: zhiyu.jiang@uia.no (Z. Jiang).

https://doi.org/10.1016/j.engfailanal.2023.107389
Received 30 April 2023; Received in revised form 23 May 2023; Accepted 4 June 2023
Available online 19 June 2023

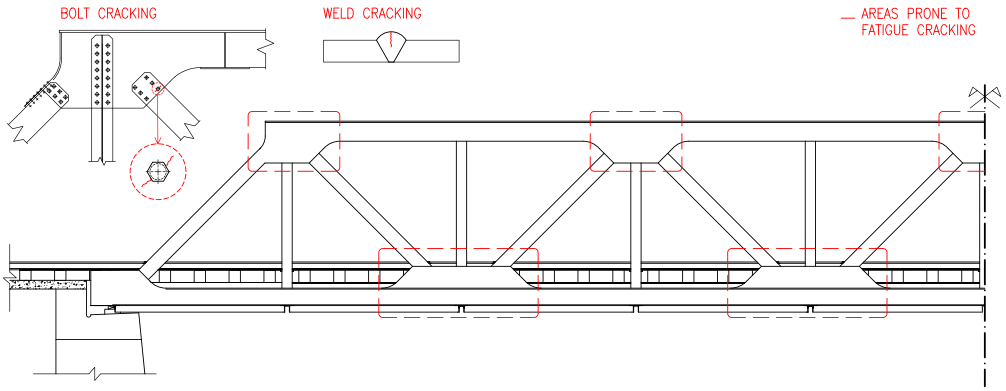

Fig. 1. Illustration of areas prone to cracking in both welded and bolted connections of Warren-type steel railway truss bridges.

To avoid premature failures of steel bridges, inspection and maintenance are necessary, and different methods exist. Visual inspection is one of the most used methods [10]. However, this method is neither cost-effective nor time-efficient. In addition, there is a risk for oversight of potential hazards. Structural health monitoring (SHM) relies on precise data measurements during operation and the measured data should be compared with base measurements to obtain useful information on structural health [11]. Research in SHM brings various alternative solutions to bridge maintenance [12,13], including computer vision-based and vibration-based methods. While the computer vision-based method [14,15] may use digital camera and artificial intelligence to localise damages, the classical vibration-based method relies on sensor measurements and considers the dynamic responses due to changes in physical aspects of bridges, such as mass and stiffness [16].

Both frequency- and time-domain approaches are widely used in vibration-based methods [17]. The frequency-domain approach examines changes in natural frequencies, mode shapes, or damping, whilst the time-domain approach directly analyses the time series of the measured acceleration and displacement signals [18]. In the following, both approaches are briefly reviewed.

Much research adopts the frequency-based vibration method for damage identification because the mass and stiffness properties affect the dynamic properties of natural frequencies and mode shapes. For example, Siriwardame [19] proposed a method for damage detection for a steel railway bridge based on modal parameters. With the proposed method, the approximate position of the damage could be determined. Kheim et al. [20] proposed a crack scanning method based on natural modes that allows identification of multiple cracks. This method can be used to identify the quantity, severity and positions of the cracks within a beam. Capecchi et al. [21] used a two-parameter objective function to identify the position and severity of the damage of a parabolic arch. This study concluded that the addition of objective function to the change in modal components can make the detection possible, as the damages are unidentifiable when comparing only the change in natural frequencies. Gorgin [22] examined the damage using the first mode shape of a beam structure. The study proposed a procedure of damage identification based on damage indices. Ay et al. [23] used a novel statistical method of probability distribution of decay rate for estimation of the modal damping ratio when comparing damage scenarios to the undamaged baseline case for a Warren-type truss bridge. This study showed the difficulties in damage identification when only the natural frequencies and mode shapes of the damaged structure are compared against those of the baseline case.

Compared with the frequency-domain approach, the time-domain approach generally derives more information from the dynamic responses of structures. With the advent of modern sensor and instrumentation technologies, signals like accelerations can easily be accessible. Teng et al. [24] used acceleration data to train a convolutional neural network to improve the accuracy of damage detection. Potenza et al. [25] presented a method for steel bridge evaluation using a combination of digital image processing and acceleration measurements. Baybordi and Esfandiari [26] proposed a new sensitivity-based updating approach based on data from time history. He et al. [27] improved the resolution of first three natural frequencies of a simply supported bridge using acceleration data from vehicle contact points. Fu et al. [28] investigated damage identifications for isotropic plate structures using a finite element model that is updated in the time domain. OBrien et al. [29] developed a damage detection method using statistical analysis of data from an acceleration-based bridge weigh-in-motion system.

In recent years, dynamic behaviours of steel truss bridges have raised interests of many researchers. Padil et al. [30] built a scaled model of a steel truss bridge in laboratory, where they created real cuttings into the truss member. Even though the scaled model and the cuttings could not represent the real scenario, their research showed the modelling and measurement error for damage detection using artificial neural network (ANN), and they proposed a non-probabilistic ANN method to address the uncertainties. Teng et al. [31] studied both a scaled laboratory model and a real steel truss bridge in order to develop a structural damage detection method based on developing digital twins and transfer learning between the numerical and real structures. Wang et al. [32] investigated a real scenario after a critical crack was found in a diagonal member near a joint of the Ikitsuki steel truss bridge and identified the causes of the crack development. Tran-Ngoc et al. [33] proposed an improved ANN method by using cuckoo search algorithm based on a study on a large-scale steel truss bridge — the Nam O Bridge. Niyirora et al. [34] recently reviewed current approaches for vibration-based damage detection and identified research gaps such as the need to optimise the sensor placement and to study damage-sensitive data other than mode shapes and natural frequencies.

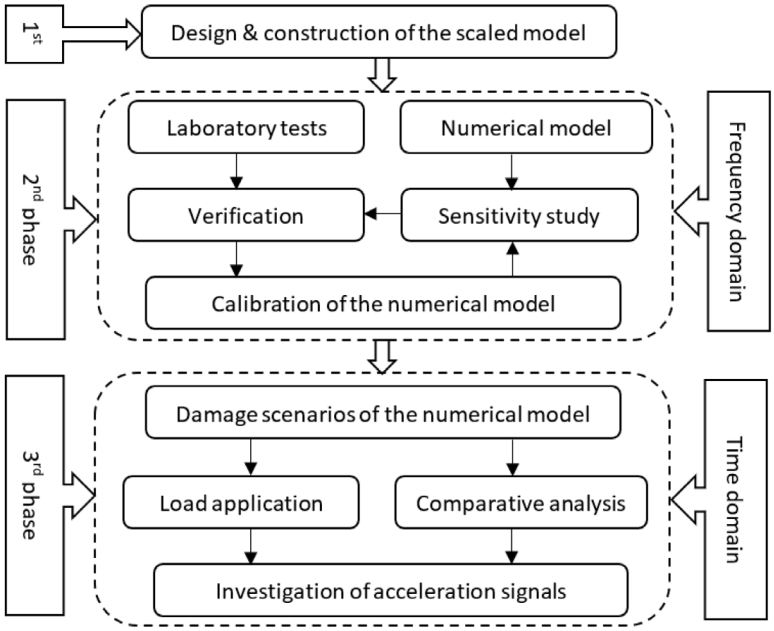

Fig. 2. Workflow of the proposed analysis procedure.

Although various methods have been proposed to identify bridge damages based on sensor measurements, there are several challenges for practical applications. On the one hand, damages are random in nature in terms of form, location and severity, and only a few sensors can be mounted on a bridge. On the other, real bridges are complex structures that change their state over time, and measurements of the initial state of many bridges in use are not available. As such, many methods are developed based on models of simple structures [21,22] where structural damages and their effects can be controlled in an easy manner.

To facilitate the development of efficient damage identification methods (e.g., damage indices, position and number of sensors) for bridges, it is necessary to have a good understanding of the bridges' dynamic behaviour under different health states, e.g., intact and damaged ones. To this end, this study concentrates on a symmetrical steel truss bridge that consists of 34 truss members. Although only a model-scale bridge is studied, its vibration features can be representative of those of realistic bridges; see [35] for example. Previously, other researchers, e.g., Padil et al. [30] and Teng et al. [31] have also studied SHM of bridges using such bridge models. To assess the effect of structural damages, we focus on the time-domain approach and carry out numerical simulations under random loads and considering various damage scenarios (crack depths and locations). Then, the dynamic response features of the bridge members are characterised. The novelty of this paper is three-fold. First, development of the time-domain approach for SHM by proposing statistical quantities to characterise the vibration signals under damage. Second, consideration of a variety of damage scenarios under random excitation. Third, comparison of acceleration response at different nodal locations to facilitate efficient deployment of sensors.

The remainder of this paper is organised as follows. Section 2 summarises the overall framework of the paper and details the material and geometry of the model bridge. Section 3 presents a verification of the established finite element model against experimentally measured data. Section 4 gives the case study with damage scenarios. Section 5 presents results and discussions for the numerical simulations. Finally, Section 6 concludes the paper with a summary.

2. Investigation framework and the case study bridge

The vibration-based method of SHM is based on the time history of vibration data signals. In order to obtain and analyse these data, the overall framework involves three phases, as shown in Fig. 2.

In the first phase, a downscaled model of a truss bridge is designed and constructed. The design considers the typical material and geometry of realistic truss bridges and also makes necessary simplifications to accommodate laboratory conditions and material availability.

In the second phase, a numerical model of the bridge is created, verified, and then calibrated based on laboratory measurements. Special attention is paid to simulation-related parameters and to calibration of fundamental natural frequencies and mode shapes.

The third phase of the study addresses damage scenarios and investigates their influences on the dynamic responses of the numerical model. Acceleration, displacement, and eigenfrequencies are considered, with the main focus on the acceleration amplitude.

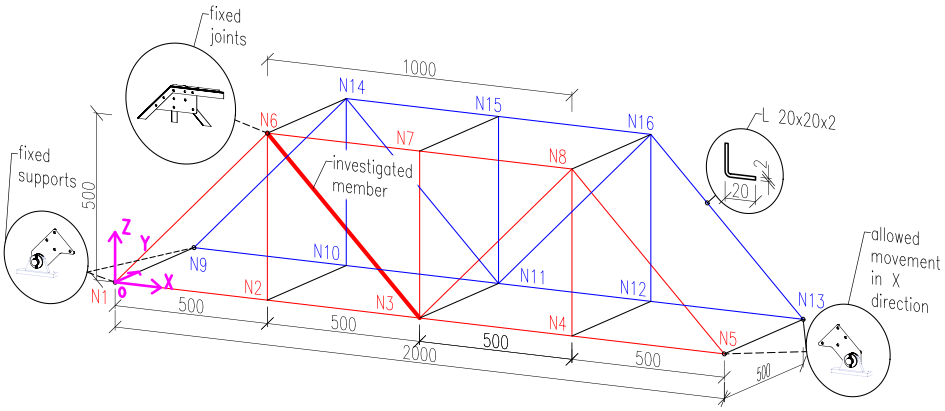

Fig. 3. Schematic of the Warren-type truss bridge.

Table 1
Characteristics of the model truss bridge.

Material		Dimensions		Truss	
Type	Steel	Length	2000 mm	Type	Warren
Young modulus	210 GPa	Width	500 mm	Supports	Simple
Poisson's ratio	0.3	Height	500 mm	Joints	Fixed

A scaled model truss bridge was designed and constructed at the structural engineering laboratory, University of Agder. Previously, a design of the bridge was carried out based on design standards [36,37] with a focus on the static load bearing criteria. Buckling check and static deflection of the bridge were addressed in a Bachelor thesis [38].

The bridge geometry consists of diagonal, vertical and horizontal trusses. This bridge is a variant of the Warren truss type which has been widely adopted in the main girder of modern suspension bridges, such as Akaishi Kaikyo Bridge, Golden Gate Bridge, and 25 de Abril Bridge. These bridges usually have a long span of kilometre level above a river or open sea. We consider this type primarily because of the difficulty to inspect these bridges using traditional methods. As shown in Fig. 3, the bridge contains 34 truss members and 16 nodes, and the model is 2000 mm long, 500 mm wide and 500 mm tall. The model was built using L-profile beams, with a cross-sectional dimension of 20 × 20 × 2 mm. The material properties of this bridge are listed in Table 1. Although standard steel and steel profiles are considered in this study [36,37], there can be uncertainties associated with the material properties and profile imperfections. For the assembled bridge, additional uncertainties arise related to boundary conditions and connections. These uncertainties should be addressed by numerical calibration.

The truss members are connected via steel brackets, each 2 mm thick, with M6 standard screws, washers and nuts. The screws are tightened with a torsional moment equal to 11 Nm. These connections are fully constrained with zero degrees of freedom (DOF). The bridge is bolted with 10-mm end brackets, and 20 mm dowel pins are used to connect the end brackets with 10-mm support brackets. Additionally, Teflon spacers are used to restrict the lateral movement between the end brackets and the support brackets. By having reamed holes in the support brackets on one side of the bridge, and slotted holes on the other side, zero translational DOF is allowed on one side, whereas one DOF on the other.

3. Numerical modelling and verification

Numerical modelling of the bridge is conducted in a finite element (FE) code, Abaqus (Version 6.14) [39]. Initially, four FE models with different fidelity levels are considered, namely beam, truss, shell, and solid elements. A good agreement among the four models is found after modal analysis, and the FE model with solid elements is further applied as it is best representative of the physical model. To calibrate the numerical model, a sensitivity study is performed to find the most suitable parameters in the numerical model.

3.1. Sensitivity study

Parameters that could significantly influence the natural frequencies include mass and stiffness properties based on the inherent relationship between them. Additionally, due to application of the FE code, the mesh size is expected to be very important. Hence, the sensitivity study is primarily carried out to select the ideal mesh size and to determine the modelling of the brackets.

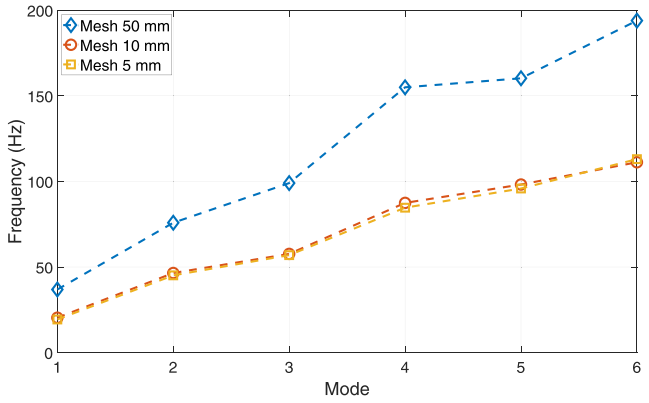

(a) Variation of the first six natural frequencies with mesh size.

Description	Physical brackets	Nodes	Numerical brackets		Size reduction
			Full	Reduced	
Boundary brackets		N1, N5, N9, N13			77.71%
Center brackets		N3, N11			80.05%
Triangular brackets		N2, N4, N7, N10, N11, N15			93.78%
Top brackets		N6, N8, N14, N16			88.70%

(b) Bracket types and the reduction process in FE analysis.

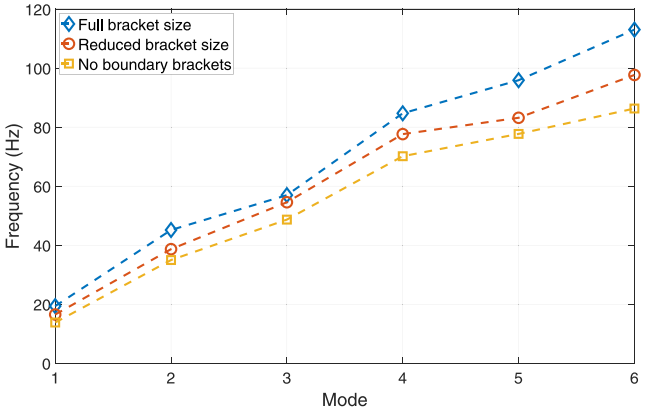

(c) Influence of the bracket size on the first six natural frequencies.

Fig. 4. Comparison of natural frequencies of the first six modes considering different settings in the FE analysis.

3.1.1. Influence of the mesh size

The whole bridge is meshed uniformly with the ten-node tetrahedral element with four integration points (C3D10 in Abaqus [39]). This element type is selected primarily because of the complicated bridge geometry.

Three mesh sizes of 5, 10, and 50 mm are investigated and Fig. 4(a) shows the damped natural frequencies of the first six modes under these mesh sizes. It can be observed that as the mesh size decreases, the natural frequencies of all modes reduce, and a significant gap exists between the 10- and 50-mm meshes. Although the average difference in the natural frequencies is approximately 43% between these two mesh sizes, the maximum difference between the 5- and 10-mm mesh size is only 3.2%.

Table 2
Summary of laboratory test conditions for modal identification.

Method	Sensor type	Excitation load	Time duration	Output data
OMA	Brüel and Kjær type 8344 piezoelectric deltashear accelerometer	Operational vibrations	60 s	Eigenfrequencies, modes and modal damping
CMA	Endevco 713-2k-240 triaxial & uniaxial piezoresistive accelerometer	Hammer	–	Eigenfrequencies, modes and modal damping

This trend is because the wall height of the L-profile is 20 mm and therefore the 5- and 10-mm mesh size equals 1/4 and 1/2 of this length, respectively, whereas the 50-mm mesh size exceeds this value. As the natural frequencies converge with the 5-mm mesh size, a further reduction in the mesh size, e.g., to 2 mm, is not considered as this would cause an exponential increase in the computational time. The final meshed bridge model consists of 188474 elements.

3.1.2. Influence of the bracket size

The bracket size in the FE model has been identified as another important factor affecting the results, because existence of the bracket affects the mass distribution of the bridge and stiffness of the connection between truss members.

In this sensitivity study, three alternatives have been considered for modelling the brackets: full brackets, reduced brackets, and reduced brackets with no boundary brackets; see Fig. 4(b) for the bracket geometries and locations. As shown in Fig. 4(c), reducing the bracket size lowers the natural frequencies. Although a reduction in the modelled bracket size causes a decrease in the structural mass, this reduction also causes a decrease in the stiffness and increases the effective length of the truss members of the bridge model, which consequently causes a decrease in the frequencies. Compared with the full bracket size, a 75%–95% reduction in the bracket size causes approximately 20% increase in the effective length of the diagonal member. This further results in a 14.8% difference in the first natural frequency, and a 13.6% difference in the sixth natural frequency. If the boundary brackets are not modelled in the FE model, the natural frequencies can decrease between 23.7–28.8% for different modes compared with the full-bracket alternative. Hence, the bracket size can be used to calibrate the FE model based on the laboratory test results.

3.1.3. Other influential factors

Other factors that influence the dynamic properties include the Young's Modulus (E), Poisson's ratio (ν), and steel density (ρ). During the calibration process, a set of values is considered for each factor, and eventually E = 200 GPa, ν = 0.29 and ρ = 7850 kg/m^3 are selected after a comparison of the obtained natural frequencies and mode shapes.

3.2. Bridge instrumentation and measurements

In order to verify the FE models considered in the sensitivity study, laboratory tests were performed together with modal identification methods. Two modal identification methods are considered here, i.e., Operational Modal Analysis (OMA) and Classical Modal Analysis (CMA).

In OMA [40], the dynamic responses of the interested structures are measured and the natural frequencies, modes and modal damping are determined. The OMA test is an output test, which means the input excitation load is not measured and its magnitude is not relevant to the results; however the exciting vibrations are considered as 'operational vibrations', as the bridge should be under normal operation when the measurements are taken.

Unlike in OMA, in CMA [41] the dynamic responses measured are excited by a measurable excitation load, typically a hammer impact. The input data are precisely measured and are considered for the output data, and the response/excitation ratio is used to determine the modal properties. The advantage of such tests is the broader range of the frequencies excited by the hammer impact.

The bridge model in the laboratory with instrumentation is shown in Fig. 5. Two types of sensors were used. As CMA does not allow sensitive sensors due to the higher magnitude of loading, three Endevco 713-2k-240 triaxial piezoresistive accelerometers [42] were used in conjunction with three Endevco uniaxial accelerometers. Their sensitivity is only 0.030 mV/ms^2, which corresponds to the test requirements. During the test, the bridge was impacted by a hammer force at the velocity of 1.14 m/s at the middle of five beams, as shown in Fig. 5. The sampling rate of the measurements is 3125 Hz.

For OMA, four piezoelectric deltashear accelerometers of type 8344 from Brüel and Kjær [41] were used. This type of accelerometer has a higher sensitivity, up to 250 mV/ms^2, which is suitable for long measurements under low vibrations. One accelerometer served as a reference sensor (see Fig. 5), whilst the other three were moved to different positions in each measurement. The vibration data were obtained in five measurements, each of 60 s time duration. The two laboratory tests with key information are summarised in Table 2.

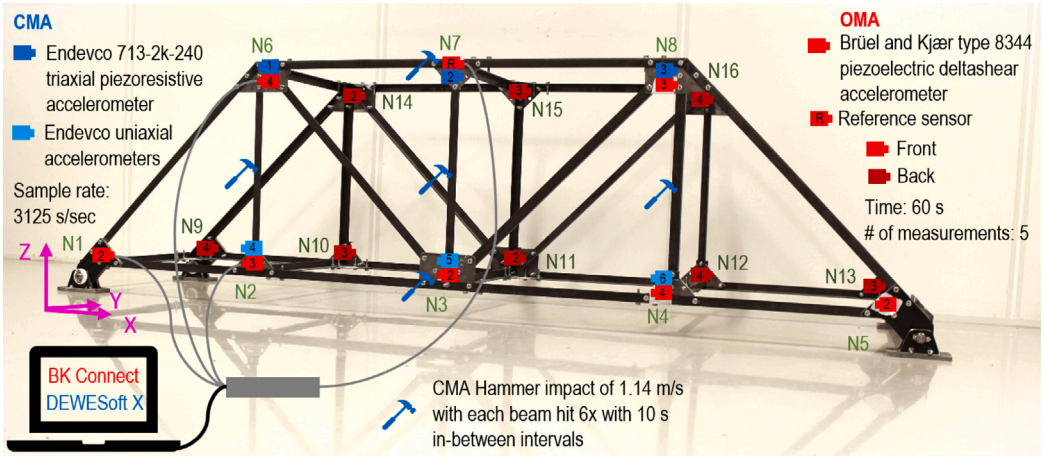

Fig. 5. Setting and instrumentation of laboratory tests.

Table 3
Results from analytical modal analysis (AMA) verified against the laboratory tests (OMA & CMA); Δ: relative difference in percentage.

Mode	AMA	OMA	Δ (%)	CMA	Δ (%)
1	16.10	15.6	3.21	15.89	1.32
2	37.71	36.1	4.46	36.59	3.06
3	53.22	45.6	16.71	46.40	14.70
4	75.76	68.0	11.41	70.27	7.81
5	81.15	79.1	2.59	81.72	−0.70
6	95.32	92.8	2.72	95.59	−0.28

3.3. Verification against laboratory tests

The present high-fidelity FE model consists of meshes of the C3D10 element type, 5-mm mesh size, Young's Modulus $E = 200$ GPa and brackets of limited size based on previous analysis in Section 3.1.

To verify the FE model, results of the numerically identified natural frequencies of six modes are compared against those identified from the laboratory tests; see Fig. 6(a). In the figure, analytical modal analysis (AMA) refers to modal analysis of the present FE model, resulting in acquisition of modal parameters such as mode shapes and natural frequencies. Compared with OMA, CMA does not consider true boundary conditions of the bridge. This can be the reason of slightly greater values of the natural frequencies measured in the CMA test.

Fig. 6(b) displays the first six eigenmodes identified by the numerical simulations. These six modes are lateral bending modes and most influential when it comes to both global dynamic responses of the entire bridge, and local responses of the diagonal members. Damage scenarios will be introduced to one diagonal member in Section 4.1. Limiting the number of the natural modes in the numerical simulations to several dominant ones is necessary to keep the computational time acceptable, and similar approaches have been adopted by Patil and Ahiwale [43] for another bridge model.

To compare the present numerical results (AMA) against the laboratory test results (OMA and CMA), we list the identified frequencies in Table 3. Compared with the identified natural frequencies from AMA, those from OMA and CMA show deviations lower than 5% for modes 1, 2, 5, and 6. Still, for modes 3 and 4, the discrepancies can exceed 10%. Such deviations can be caused by various uncertainty factors related to both the physical and numerical models. Overall, the calibrated FE model is deemed acceptable for further simulations in this study.

4. Case study

The case study consists of two subsets of damage scenarios. The first subset considers different damage locations, whilst the second subset considers different damage severity.

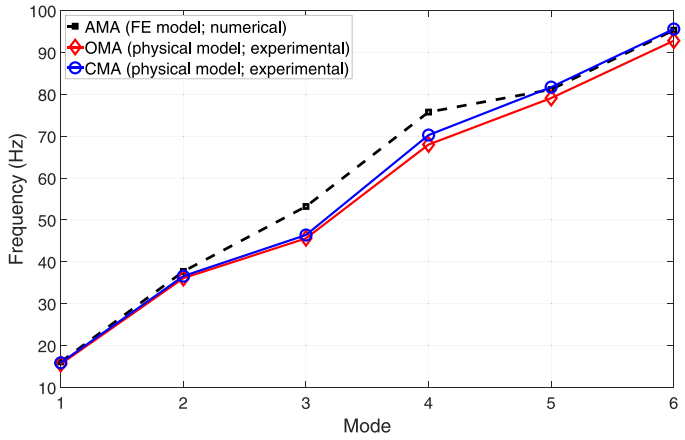

(a) Comparison of results of the first six modes obtained from the sensitivity study to the results obtained from laboratory tests.

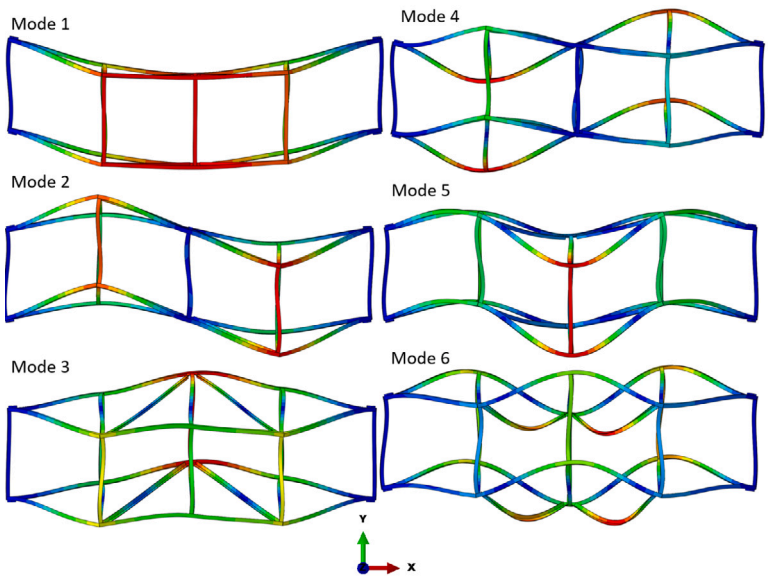

(b) Mode shapes of the first six modes considered in this study.

Fig. 6. Verification of the numerical model against the laboratory tests.

4.1. Damage scenarios

The diagonal member (M7, see Fig. 7(a)) is chosen for all the damage scenarios due to the influence of the damage of this member on the loss of stiffness of the entire bridge. The initial damages consist of three damage cases listed in Table 4. The damage cases have the same crack geometry with different locations. Each crack is 10 mm deep and 0.5 mm wide, cutting through the thickness of the L-profile. This damage depth represents 50% of the wall thickness. Case 'B' has the crack in the middle of the diagonal member, and the other two cases have the crack 300 mm off the midpoint. These two damages are positioned very close to the reduced brackets on each side, at a distance of approximately 3.5 mm. After determining the effect of each damage location, additional damage cases consisting of damage with different depths were considered at the most responsive location (see Table 4). The severity of the damage considered ranged from 10 to 50%, i.e., from 2 to 10 mm.

Compared with the mesh size of the intact bridge, a finer mesh size of 0.5 mm was used at the edges of all crack-like damages, as shown in Fig. 7(b).

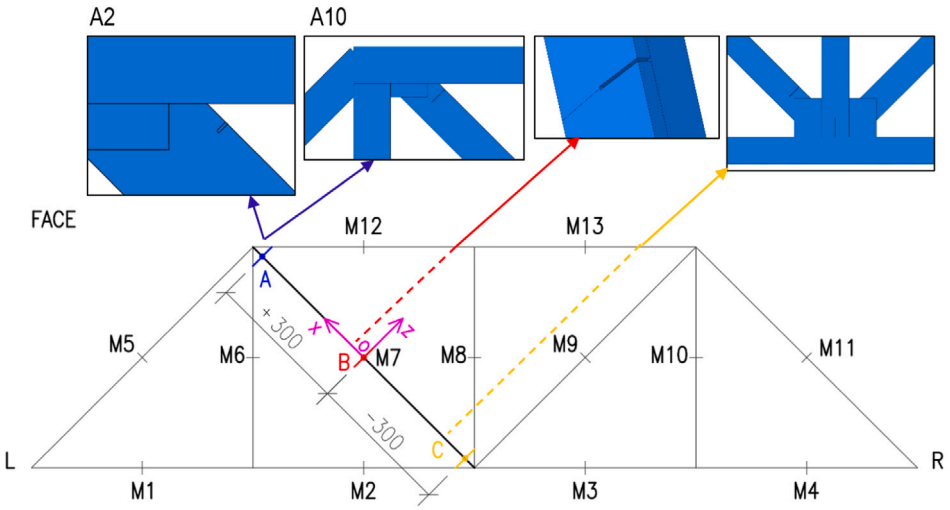

(a) The front side of the bridge with damage scenarios.

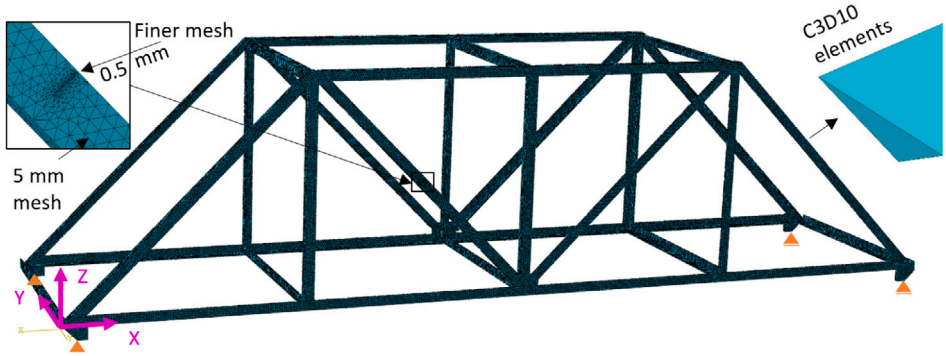

(b) The meshed finite element model with a crack.

Fig. 7. Illustration of the bridge model in the case study.

Table 4
List of the studied damage cases with various location and severity.

Damage case	Damage depth		Position (from M7)	Damage case	Damage depth		Position (from M7)
	Relative	Actual			Relative	Actual	
A	50%	10 mm	300 mm	A2	10%	2 mm	300 mm
B	50%	10 mm	0 mm	A4	20%	4 mm	300 mm
C	50%	10 mm	−300 mm	A6	30%	6 mm	300 mm
				A8	40%	8 mm	300 mm
				A10	50%	10 mm	300 mm

4.2. Time-domain response to the white noise loading

4.2.1. Modal dynamic analysis

Generally, a structural system subjected to dynamic loads can be expressed by the following equation of motion (EOM).

$$\mathbf{m}\ddot{\mathbf{u}}(t) + \mathbf{c}\dot{\mathbf{u}}(t) + \mathbf{k}\mathbf{u}(t) = \mathbf{f}(t) \tag{1}$$

where $\mathbf{m}, \mathbf{c}$ and $\mathbf{k}$ are the mass, damping and stiffness matrices of a structure, and $\ddot{\mathbf{u}}, \dot{\mathbf{u}}$ and $\mathbf{u}$ are acceleration, velocity and displacement vectors, respectively. $\mathbf{f}$ is the vector of the external load.

There are several methods for performing dynamic analysis of structural systems, including direction integration methods and modal methods [44]. Considering the linear nature of the bridge system and computational efficiency, we chose modal dynamic analysis to obtain the dynamic responses in the time domain using modal superposition. This approach has been applied in similar studies where stochastic loading is used for structures [45,46].

Because the modal dynamic approach bases the structure's response on the modes of the system, a frequency extraction procedure must be performed first [39]. Accordingly, the six selected modal frequencies and shapes are extracted based on the previous results. With the consideration of modal damping and time-dependent loading, the EOM can be expressed as Eq. (2).

$$\ddot{\mathbf{q}} + 2\xi\omega\dot{\mathbf{q}} + \omega^2\mathbf{q} = \mathbf{f}_t = \mathbf{f}_{t-\Delta t} + \frac{\Delta \mathbf{f}}{\Delta t}\Delta t \tag{2}$$

where $\mathbf{q}$ is the amplitude of the response in a mode; ξ is the damping ratio; ω is the natural frequency of the undamped mode; $\mathbf{f}$ is the magnitude of the loading projected onto the mode and Δt is the time increment.

4.2.2. Damping effects

The damping effects in modal dynamics are considered through the damping ratio ξ. In this study, the damping ratio is determined based on the experimentally obtained data by investigating the reduction of amplitude peaks and is found to be 0.98%. Here, the same damping ratio is included for all six modes in the modal dynamic analysis.

4.2.3. Simulation length

In order to obtain results that include the first six eigenmodes in the range of 0–100 Hz, a time increment of 0.005 s was applied in the time-domain simulation of the bridge. This increment was chosen primarily because of computational efficiency. To determine the simulation length for the case study, we compared the results of three simulation length, i.e., 10, 30, and 60 s, for the undamaged bridge model subjected to white noise loading. Although the length of the time history has an effect on the statistics of interested responses, e.g., acceleration, the overall trends and general observations of the damages' effect remain the same. For the sake of computational efficiency, the simulation length for all damage scenarios is kept at 10 s.

4.2.4. White noise loading

In the time-domain numerical simulations, a stochastic load in the form of white noise is applied on the bridge to excite random vibrations of the structure. The white noise loading condition is a wide-band excitation representative of ambient conditions with wind and temperature effects. Such conditions have been considered by others [47]. For real bridges, the load effect from traffic loads [48] should also be properly considered. As shown in Fig. 8(a), the pre-generated time series of white noise load has small amplitudes to ensure that the material behaviour of the bridge is linear-elastic. On the other hand, the load covers a broad frequency range of 0–100 Hz after performing a Fourier transform of the auto-correlation function [49]; see Fig. 8(b). This point load is applied at the $N3$ node in the y-direction (Fig. 3). The position of the load was chosen such that the load would influence the diagonals symmetrically.

5. Results and discussions

In this section, the dynamic responses of each member as well as the overall model are analysed with a focus on the acceleration response. The results of damaged models are compared with those of the intact model in order to quantify the influence of the damage. The discussion follows the order of damage location, severity and finally, the influence of pseudo noise.

5.1. Effect of the damage location on dynamic responses

First, the results obtained from the midpoints of all 34 bridge members are investigated. Then, seven additional points on the damaged member are compared. In addition to the midpoints, nodal points are also considered due to their high displacement in the six mode shapes (see Fig. 6(b)). As the influence of damage on the nodal points is limited, the results are not presented.

5.1.1. Comparison of midpoints responses

As illustrated in Fig. 9, one midpoint from each member of the bridge is initially investigated. These points are chosen because of their positions on the local axis of symmetry and hence their high sensitivity to external loading and changes in structural properties of the bridge.

As the damages (case A–C) affect the mass and stiffness properties of the diagonal member, the accelerations of all midpoints experience differences. Fig. 10 shows one representative time series of a nodal acceleration under two circumstances. As shown, the time series is of stationary and stochastic nature under the white noise excitation. The blue curve (damage case C) has increased envelope than the red curve (undamaged), but the differences are relatively small at any time instant. To measure the differences, we considered several statistics and found the root mean square (RMS) of the entire time series to be an effective metric of the cumulative differences.

$$acc_{mag} = \sqrt{acc_x^2 + acc_y^2 + acc_z^2} \tag{3}$$

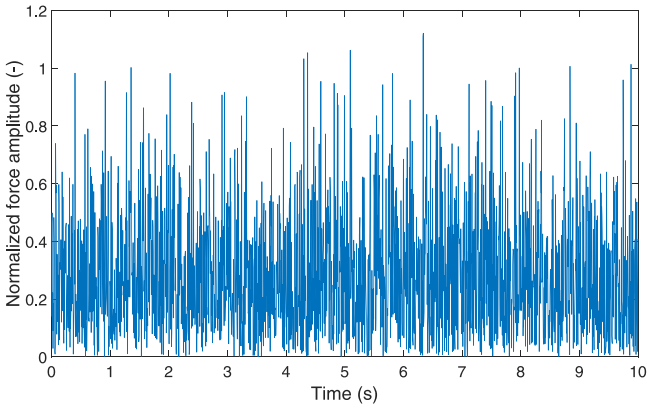

(a) Time history of the normalized force amplitude, with normalized force 1 = 10 N.

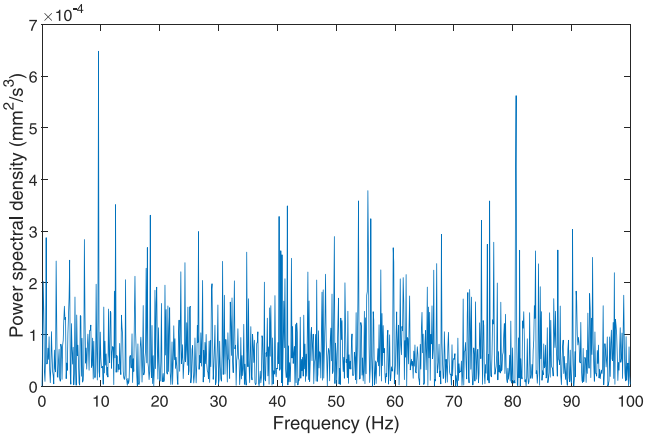

(b) Power spectral density of acceleration results.

Fig. 8. Properties of the white noise loading, which was set in the numerical model.

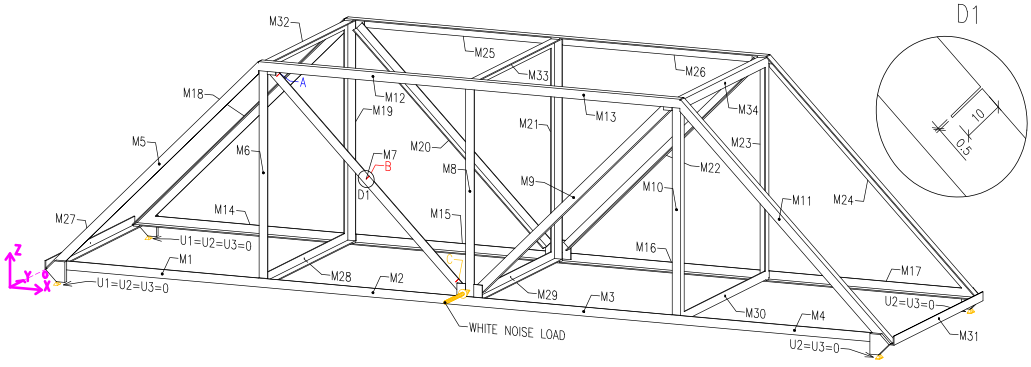

Fig. 9. Illustration of the 34 midpoints (M1–M34) whose dynamic responses are initially investigated.

Fig. 11(a) presents the absolute difference of the RMS magnitudes between the three damaged cases and the undamaged case. The magnitude results are obtained from Eq. (3). Generally, the damage case B causes much less changes than the damage cases A and C. This observation can be explained by the fact that a crack close to a bolt connection affects more the local boundary support of the diagonal member than a crack away from a connection.

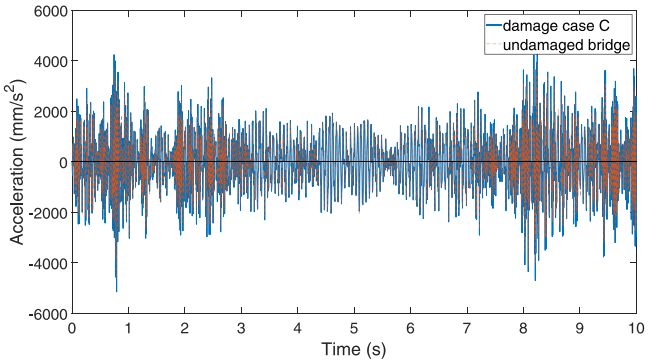

Fig. 10. Selected acceleration time history of the midpoint M7 in the Y-direction, damage case C.

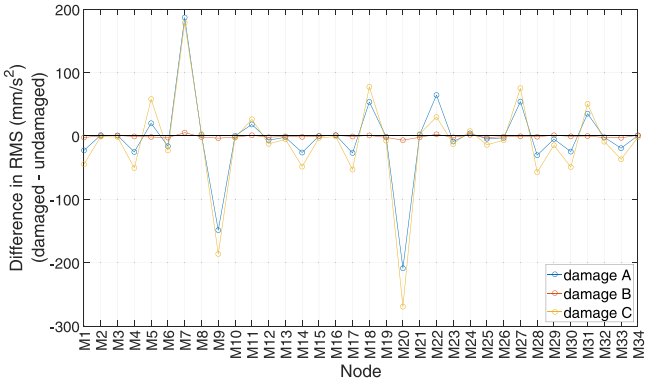

(a) Difference of the RMS of the total acceleration magnitude between a damaged case and the undamaged case for 34 midpoints; damage case A–C.

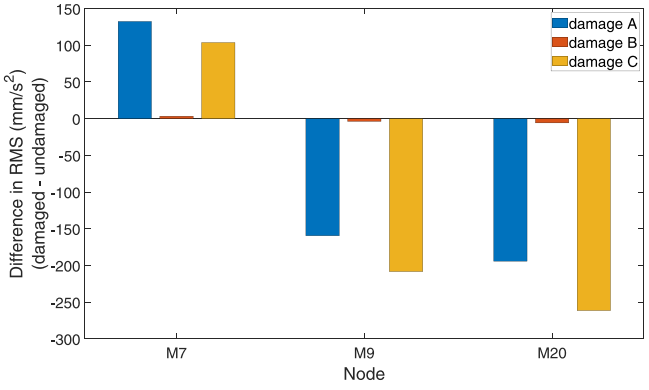

(b) Difference of the RMS of the Y-acceleration of between a damaged case and the undamaged case for three midpoints; damage case A–C.

Fig. 11. Results from initially investigated points of the scaled bridge numerical model.

Among the investigated midpoints, the most significant changes are observed for M7, M9 and M20. Take the damage case C for example. The relative percentage change is 15.5%, 17.3%, and 23.4% for M7, M9, and M20, respectively. Considering the spatial positions of these three points, M9 and M20 can be regarded as two symmetric points of M7. Interestingly, after a crack damage is brought to the model, these points have different trends in the RMS magnitude, which increases for M7 but decreases for M9 and M20. This observation indicates that the dynamic response of a nodal acceleration is more complicated than that of the static

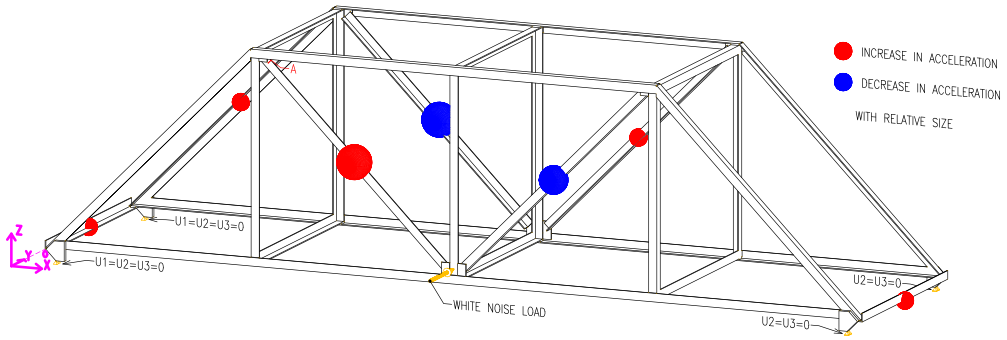

Fig. 12. Changes in acceleration responses of the bridge due to the damage 'A' with red showing an increase and blue decrease; and the relative size showing the size of the difference.

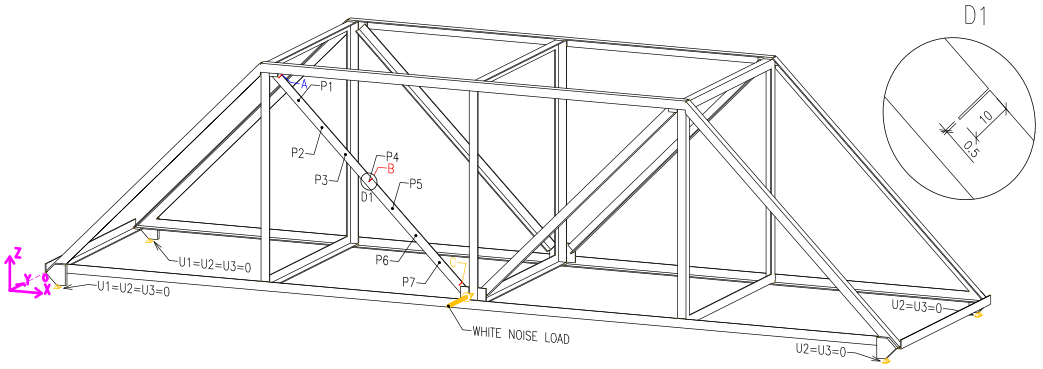

Fig. 13. Additional seven points (P1–P7) investigated on the damaged diagonal member.

response of a nodal displacement upon the presence of a crack. While the displacement is expected to increase because of the reduced structural stiffness induced by a crack, accelerations at different nodal positions of the bridge do not necessarily increase, as can be inferred by Eq. (2). A crack causes reduction in both the inertia and stiffness terms which further complicates the natural frequencies of global modes and the dynamic responses. As M7 is located on the diagonal member where damages are imposed, its acceleration appears to have a higher overall magnitude than any other investigated midpoints.

In addition to M7, M9, and M20, other 31 midpoints are analysed considering the differences in the acceleration RMS. As M18 and M22 are located on two diagonal members away from the damaged member (see Fig. 9), these two points encounter limited increase in the RMS magnitude of acceleration. Some small differences are also reported for the members between the two sets of supports.

As RMS of the total acceleration magnitude only considers the summed effect in three directions, the effects of damages on responses in the X-, Y- and Z-directions are further studied. It is found that the most dominant component in the acceleration magnitude is from the Y-direction. This observation is expected because the white noise loading is pointed in the Y-direction which directly affects the dynamic responses in that direction. As shown in Fig. 11(b), the RMS differences of the Y- acceleration have similar trends as those of the total acceleration after damages are brought to the model, and damage cases A and C have stronger effects than damage case B.

To visualise the effect of damages and the direction of the change in the acceleration magnitudes, we plot red or blue spheres for selected midpoints in Fig. 12. Here, the larger the sphere, the higher impact on the nodal acceleration.

These findings opens up opportunities for efficient SHM considering sensor deployment and damage detection. For similar truss bridges, the midpoints of the crossbars between the supports can be measured first. If there is an appreciable difference in the acceleration RMS, additional points can be investigated to locate the crack position.

5.1.2. Comparison of responses on the damaged member

Because the midpoint of the damaged diagonal member experiences a significant increase in the measured acceleration, the damaged diagonal member is investigated more closely. The RMS of the total acceleration magnitude of seven points, P1–P7, are considered. Among these points, P4 is close to the midpoint, and P1 and P7 are close to the end connections; see Fig. 13. As shown in Fig. 14, regardless of the damage cases, the variation trend of the RMS difference with the seven points is almost bell-shaped due to the symmetry of the points with regard to midpoint. Another observation is that the location of the cracks (i.e., damage cases A–C) does not affect the variation trend in the RMS, but influences more the magnitude of the RMS difference. As we only

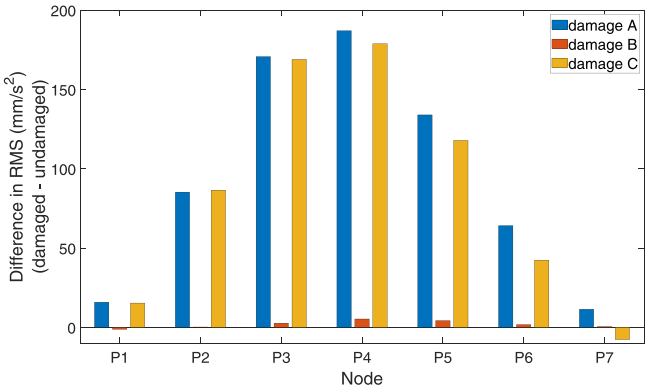

Fig. 14. Results of difference in RMS of accelerations of 7 additionally investigated points.

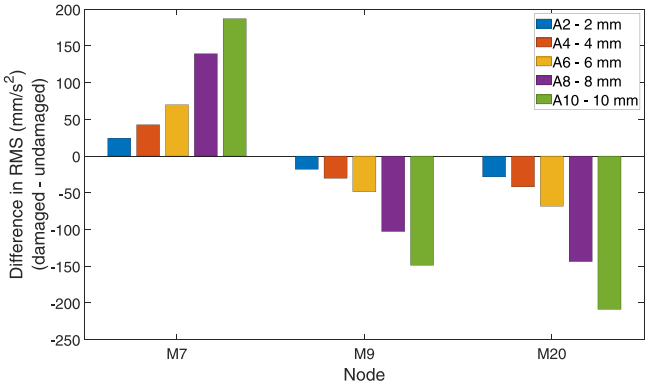

Fig. 15. Differences in the acceleration RMS of five damage scenarios with different damage severity.

considered six lateral bending modes in the frequency extraction (see Section 4.2.1), it is possible that the acceleration magnitudes and the corresponding RMS may change if additional modes are considered in modal dynamic analysis. For this reason, additional time-domain numerical simulations were carried out with a broader spectrum of natural frequencies. In the simulations where the first 50 eigenmodes are considered, the acceleration magnitudes of the seven points remain at the same level and the observations of the RMS trend still hold. Based on these results, we can conclude that the considered six lateral bending modes have a large influence on the acceleration of the damaged member although the precise position of the crack-like damage may be hard to locate by measuring the changes in acceleration on this type of steel bridge.

5.2. Influence of damage severity on the dynamic responses

The initial damage scenarios (case A–C) have a relative depth of damage 50%, which could be considered a severe case. In the study of the influence of damage severity, five damage cases (A2–A10) are considered (see Table 4) with the relative depth ranging from 10% to 50% at an increment of 10%. The position 'A' is chosen as the location to investigate damages of different severity. Based on previous analysis, this location is expected to have significant effect on the dynamic responses.

For damages with a depth of less than 6 mm, the difference in RMS of acceleration is less than 50 mm/s^2, which represents a 2.72% change from the RMS of the undamaged case; see Fig. 15. If a longer time duration than 10 s is considered in the simulations, the absolute difference in the RMS of acceleration is expected to increase and exceed 50 mm/s^2. This value is taken as the threshold in this study, while it should be decided based on numerical analysis for different bridges. Still, a similar level of relative difference (damaged versus undamaged) should remain because of the stationary nature of the response. If only damages of great magnitudes could be identified on the basis of these results, then damages of relative depths less or equal to 30% could be found undetectable in this scenario. These results are expected because the relatively small depth of the damage has only a minor influence on the stiffness of the bridge, which results in a minor change in the natural frequencies, accelerations and other dynamic responses.

5.3. Influence of noise on acceleration responses

In real-life scenarios, the measured acceleration signals of a bridge may contain noises from various sources [50]. To address this aspect, additional noises are added to the original acceleration signals from the numerical simulations. Here, the additive white

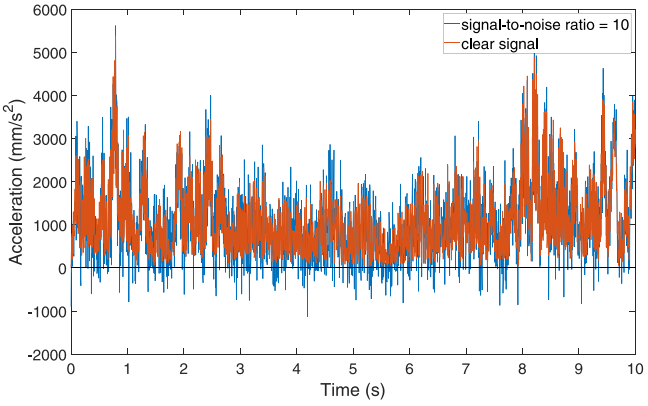

(a) Magnitude acceleration signal from damage 'A' point M7 with a pseudo noise of SNR=10, damage case A.

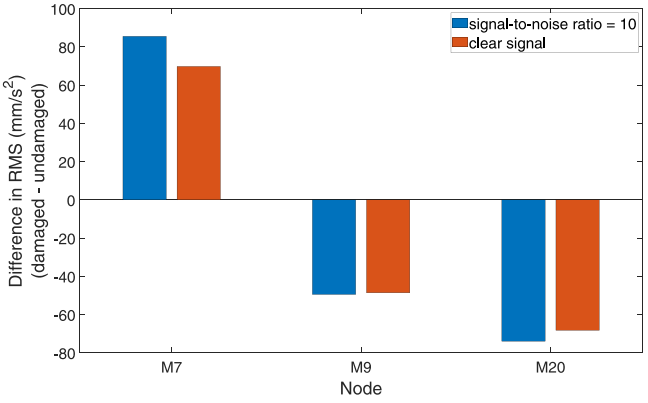

(b) Difference in the acceleration RMS of three midpoints, damage case A.

Fig. 16. Differences in acceleration results of chosen points with addition of pseudo noise in a form of white Gaussian noise in comparison with the clear results.

Gaussian noise to signal [51] is used to create a pseudo noise. The modified acceleration signal with pseudo noise is expressed in Eq. (4) as follows.

$$Y(t) = X(t) + Z(t) \tag{4}$$

where $Y(t)$ is the modified acceleration signal, $X(t)$ is the original, clear acceleration signal, and $Z(t)$ is the noise signal generated with power spectral density $\mathcal{N}_0$ [51]. $X(t)$ and $Z(t)$ are independent processes.

The signal-to-noise ratio (SNR), is a measure of the strength of the clear signal relative to background noise (undesired signal). SNR is computed as the ratio of the summed squared magnitude of $X(t)$ to that of the noise, $Z(t)$. Various pseudo noises with different SNRs are generated and added to the acceleration signals. Fig. 16(a) compares the time series for acceleration at M7 for damage case A. In this case, although the considered noise level is quite low with an SNR of 10, noticeable differences in the acceleration signal can be observed.

For damage detection, a practical threshold for the RMS difference of 50 mm/s^2 can be assumed. Previously, similar approaches were suggested for the serviceability of highway bridges in Japan [52]. When SNR is greater than 2, damages with a crack depth of more than 8 mm (40% relative depth) can be considered detectable. If SNR equals 10, damages with a crack depth of 6 mm (30% relative depth) is the smallest crack that could be detected. Considering the fact that SNR may vary between 2 and 20 in many real-life scenarios, damage detection of cracks at their early development stages is a challenge.

The differences in the acceleration RMS with and without the pseudo noise are shown in Fig. 16(b). Although these three midpoints show an increase in the RMS difference after the noise is added, the observed trend can be opposite if a different pseudo noise is considered. Because the noise itself is Gaussian and generated with a random seed number, the noise brings uncertainties to the measurements and causes difficulties for damage detection in practice. Among the three midpoints, M7 is still the point whose acceleration response is most appreciable after a damage is introduced.

6. Conclusion

This study deals with the dynamic responses of a scaled truss bridge due to damages. A high-fidelity numerical model is first calibrated with a sensitivity study based on laboratory tests. The influence of mesh size and bracket dimensions is considered, as well as the overall stiffness of the bridge. Then, damage scenarios addressing various crack depth and location are considered for a diagonal member. Finally, the dynamic responses of the damaged bridge are compared with those of the undamaged bridge, and influential factors that may affect damage detection are discussed. The following main conclusions are drawn:

(a) When verifying the numerical bridge model against the physical one, uncertainties brought by instrumentation and boundary conditions should be considered. For a truss bridge, the effective length of a member in the numerical model may differ from that of a real one.
(b) A significant increase in acceleration can be found for the damaged member, whereas small differences for other members. Decrease in the acceleration root mean square (RMS) can be observed for diagonal members symmetrical to the damaged member. The relationship between damages and accelerations is complex. These results indicate that the damaged member of the steel truss bridge could be identified using vibration-based approaches.
(c) There is a high percentage increase in accelerations in points near the supports. Even though the actual acceleration value is quite low, this observation opens up the possibility of using a few measurements to determine the overall structural health of a truss bridge.
(d) Midpoints of truss members are most sensitive in acceleration to damages. The damages could be potentially found if accelerations of the midpoint of a damaged member displays substantially more increases in RMS than other members.
(e) When adding pseudo white Gaussian noise to the original acceleration signals, only damages with large crack depths, e.g., $\geq$ 30%, can have detectable differences in the acceleration signals.

7. Limitation and future work

This paper focuses on computational modelling of the dynamic responses of a model bridge due to crack-like damages. Due to limitation of time and resources, the experimental results are used to verify the computational model of the intact bridge. During the time-domain numerical simulations, only a simplified white noise loading is considered.

In future, the following aspects can be considered based on the present research outcomes:

- Comparison of the dynamic behaviours of the model truss bridge against similar full-scale bridges.
- Development of damage identification methods and monitoring strategies.
- Development of efficient, frequency-domain approaches and comparison against time-domain ones.
- Enhancement of vibration-based approaches by loading tests which can load the target bridge by vehicles and can provide global flexural stiffness of the bridge.

Declaration of competing interest

The authors declare that they have no known competing financial interests or personal relationships that could have appeared to influence the work reported in this paper.

Data availability

Data will be made available on request.

Acknowledgements

The visiting scholar scholarship granted by University of Agder, Norway is gratefully acknowledged by the first author.

References

[1] EN 1994-2, Eurocode 1 - Actions on structures - Part 2: Traffic loads on bridges, Tech. Rep, CEN, 2003.
[2] Z. Sun, J. Santos, E. Caetano, Data-driven prediction and interpretation of fatigue damage in a road-rail suspension bridge considering multiple loads, Struct. Control Health Monit. 29 (9) (2022) e2997.
[3] L. Deng, W. Wang, Y. Yu, State-of-the-art review on the causes and mechanisms of bridge collapse, J. Perform. Constr. Facil. 30 (2) (2016) 04015005, http://dx.doi.org/10.1061/(ASCE)CF.1943-5509.0000731.
[4] M. Simoncelli, A. Aloisio, M. Zucca, G. Venturi, R. Alaggio, Intensity and location of corrosion on the reliability of a steel bridge, J. Construct. Steel Res. 206 (March) (2023) 107937, http://dx.doi.org/10.1016/j.jcsr.2023.107937.
[5] G. Zhang, Y. Liu, J. Liu, S. Lan, J. Yang, Causes and statistical characteristics of bridge failures: A review, J. Traffic Transp. Eng. (Engl. Ed.) 9 (3) (2022) 388–406, http://dx.doi.org/10.1016/j.jtte.2021.12.003.
[6] C. Klinger, T. Michael, D. Bettge, Fatigue cracks in railway bridge hangers due to wind induced vibrations - Failure analysis, measures and remaining service life estimation, Eng. Fail. Anal. 43 (2014) 232–252, http://dx.doi.org/10.1016/j.engfailanal.2014.02.019.
[7] H. Tan, X. Hu, X. Wu, Y. Zeng, X. Tu, X. Xu, J. Qian, Initial crack propagation of integral joint in steel truss arch bridges and its fatigue life accession, Eng. Fail. Anal. 130 (July) (2021) 105777, http://dx.doi.org/10.1016/j.engfailanal.2021.105777.

[8] R. Haghani, M. Al-Emrani, M. Heshmati, Fatigue-prone details in steel bridges, Buildings 2 (4) (2012) 456–476, http://dx.doi.org/10.3390/buildings2040456.

[9] S.B. Lee, Fatigue failure of welded vertical members of a steel truss bridge, Eng. Fail. Anal. 3 (2) (1996) 103–108, http://dx.doi.org/10.1016/1350-6307(96)00003-9.

[10] Z. Sun, D. Siringoringo, Z. Chen, J. Lu, Cumulative displacement-based detection of damper malfunction in bridges using data-driven isolation forest algorithm, Eng. Fail. Anal. 143 (PB) (2023) 106849, http://dx.doi.org/10.1016/j.engfailanal.2022.106849.

[11] P. Cawley, Structural health monitoring: Closing the gap between research and industrial deployment, Struct. Health Monit. 17 (5) (2018) 1225–1244, http://dx.doi.org/10.1177/1475921717750047.

[12] Z. Sun, Z. Zou, Y. Zhang, Utilization of structural health monitoring in long-span bridges: case studies, Struct. Control Health Monit. 24 (10) (2017) e1979.

[13] R. Zaurin, F.N. Catbas, Integration of computer imaging and sensor data for structural health monitoring of bridges, Smart Mater. Struct. 19 (1) (2009) 015019, http://dx.doi.org/10.1088/0964-1726/19/1/015019.

[14] R. Nigam, S.K. Singh, Crack detection in a beam using wavelet transform and photographic measurements, Structures 25 (October 2019) (2020) 436–447, http://dx.doi.org/10.1016/j.istruc.2020.03.010.

[15] S. Patsias, W.J. Staszewski, Damage detection using optical measurements and wavelets, Struct. Health Monit. 1 (1) (2002) 5–22, http://dx.doi.org/10.1177/147592170200100102.

[16] O. Markogiannaki, A. Arailopoulos, D. Giagopoulos, C. Papadimitriou, Vibration-based damage localization and quantification framework of large-scale truss structures, Struct. Health Monit. (2022) 1–23, http://dx.doi.org/10.1177/14759217221100443.

[17] M. Muñiz-Calvente, A. Álvarez-Vázquez, F. Pelayo, M. Aenlle, N. García-Fernández, M.J. Lamela-Rey, A comparative review of time- and frequency-domain methods for fatigue damage assessment, Int. J. Fatigue 163 (May) (2022) 107069, http://dx.doi.org/10.1016/j.ijfatigue.2022.107069.

[18] Y. Yang, Y. Zhang, X. Tan, Review on vibration-based structural health monitoring techniques and technical codes, Symmetry 13 (11) (2021) 1–18, http://dx.doi.org/10.3390/sym13111998.

[19] S.C. Siriwardane, Case studies in engineering failure analysis vibration measurement-based simple technique for damage detection of truss bridges : A case study, Case Stud. Eng. Fail. Anal. 4 (2015) 50–58, http://dx.doi.org/10.1016/j.csefa.2015.08.001.

[20] N.T. Khiem, H.T. Tran, A procedure for multiple crack identification in beam-like structures from natural vibration mode, J. Vib. Control 20 (9) (2014) 1417–1427, http://dx.doi.org/10.1177/1077546312470478.

[21] D. Capecchi, J. Ciambella, A. Pau, F. Vestroni, Damage identification in a parabolic arch by means of natural frequencies, modal shapes and curvatures, Meccanica 51 (11) (2016) 2847–2859, http://dx.doi.org/10.1007/s11012-016-0510-3.

[22] R. Gorgin, Damage identification technique based on mode shape analysis of beam structures, Structures 27 (August) (2020) 2300–2308, http://dx.doi.org/10.1016/j.istruc.2020.08.034.

[23] A.M. Ay, S. Khoo, Y. Wang, Probability distribution of decay rate: a statistical time-domain damping parameter for structural damage identification, Struct. Health Monit. 18 (1) (2019) 66–86, http://dx.doi.org/10.1177/1475921718817336.

[24] S. Teng, G. Chen, Z. Liu, L. Cheng, X. Sun, Multi-sensor and decision-level fusion-based structural damage detection using a one-dimensional convolutional neural network, Sensors 21 (12) (2021) http://dx.doi.org/10.3390/s21123950.

[25] F. Potenza, G. Castelli, V. Gattulli, E. Ottaviano, Integrated process of images and acceleration measurements for damage detection, Procedia Eng. 199 (2017) 1894–1899, http://dx.doi.org/10.1016/j.proeng.2017.09.126.

[26] S. Baybordi, A. Esfandiari, A novel sensitivity-based finite element model updating and damage detection using time domain response, J. Sound Vib. 537 (June) (2022) 117187, http://dx.doi.org/10.1016/j.jsv.2022.117187.

[27] Y. He, J.P. Yang, Using acceleration residual spectrum from single two-axle vehicle at contact points to extract bridge frequencies, Eng. Struct. 266 (May) (2022) http://dx.doi.org/10.1016/j.engstruct.2022.114538.

[28] Y.Z. Fu, Z.R. Lu, J.K. Liu, Damage identification in plates using finite element model updating in time domain, J. Sound Vib. 332 (26) (2013) 7018–7032, http://dx.doi.org/10.1016/j.jsv.2013.08.028.

[29] E. OBrien, M.A. Khan, D.P. McCrum, A. Žnidarič, Using statistical analysis of an acceleration-based bridgeweigh-in-motion system for damage detection, Appl. Sci. (Switzerland) 10 (2) (2020) http://dx.doi.org/10.3390/app10020663.

[30] K.H. Padil, N. Bakhary, M. Abdulkareem, J. Li, H. Hao, Non-probabilistic method to consider uncertainties in frequency response function for vibration-based damage detection using Artificial Neural Network, J. Sound Vib. 467 (2020) 115069, http://dx.doi.org/10.1016/j.jsv.2019.115069.

[31] S. Teng, X. Chen, G. Chen, L. Cheng, Structural damage detection based on transfer learning strategy using digital twins of bridges, Mech. Syst. Signal Process. 191 (September 2022) (2023) 110160, http://dx.doi.org/10.1016/j.ymssp.2023.110160.

[32] Q. Wang, S. Nakamura, T. Okumatsu, T. Nishikawa, Comprehensive investigation on the cause of a critical crack found in a diagonal member of a steel truss bridge, Eng. Struct. 132 (2016) 659–670, http://dx.doi.org/10.1016/j.engstruct.2016.11.049.

[33] H. Tran-Ngoc, S. Khatir, G. De Roeck, T. Bui-Tien, M. Abdel Wahab, An efficient artificial neural network for damage detection in bridges and beam-like structures by improving training parameters using cuckoo search algorithm, Eng. Struct. 199 (February) (2019) 109637, http://dx.doi.org/10.1016/j.engstruct.2019.109637.

[34] R. Niyirora, W. Ji, E. Masengesho, J. Munyaneza, F. Niyonyungu, R. Nyirandayisabye, Intelligent damage diagnosis in bridges using vibration-based monitoring approaches and machine learning: A systematic review, Res. Eng. 16 (October) (2022) 100761, http://dx.doi.org/10.1016/j.rineng.2022.100761, URL https://doi.org/10.1016/j.rineng.2022.100761.

[35] Y. Liang, D. Li, G. Song, Q. Feng, Frequency Co-integration-based damage detection for bridges under the influence of environmental temperature variation, Measurement 125 (2018) 163–175.

[36] EN 1993-1, Eurocode 3: Design of Steel Structures - General Rules and Rules for Buildings, Tech. Rep., CEN, 2005.

[37] EN 1993-2, Eurocode 3 - Design of steel structures - Part 2: Steel Bridges, Tech. Rep., CEN, 2006.

[38] M. Awale, M. Rai, O.-E. Odinson, Construction, numerical modelling, and static testing of a downscaled steel truss bridge (Bachelor thesis), Department of Engineering Sciences, University of Agder, Grimstad, Norway, 2022.

[39] D. Systèmes, Abaqus Analysis User's Guide, Version 6.14 in Dassault Systèmes, Simulia, Rhode Island, United States, 2014.

[40] E. Reynders, G.D. Roeck, Reference-based combined deterministic-stochastic subspace identification for experimental and operational modal analysis, Mech. Syst. Signal Process. 22 (3) (2008) 617–637, http://dx.doi.org/10.1016/j.ymssp.2007.09.004.

[41] B.. Kjær, Classical Modal Analysis. URL https://www.bksv.com/en/knowledge/applications/structural-dynamics/modal-analysis.

[42] ENDEVCO, Data sheet for ENDEVCO 713-2k-240. URL https://buy.endevco.com/ContentStore/MktgContent/Endevco/Datasheet/713-713F_DS_083019.pdf.

[43] V. Patil, D. Ahiwale, Damage detection of warren truss bridge using frequency change correlation, Mater. Today: Proc. 56 (2022) 18–28, http://dx.doi.org/10.1016/j.matpr.2021.11.483.

[44] R.R. Craig Jr., A.J. Kurdila, Fundamentals of Structural Dynamics, John Wiley & Sons, 2006.

[45] W.X. Ren, H.B. Chen, Finite element model updating in structural dynamics by using the response surface method, Eng. Struct. 32 (8) (2010) 2455–2465, http://dx.doi.org/10.1016/j.engstruct.2010.04.019.

[46] S.M.M. Randiligama, D.P. Thambiratnam, T.H. Chan, S. Fawzia, K. Duy Nguyen, Vibration based damage detection in hyperbolic cooling towers using coupled method, Eng. Fail. Anal. 121 (December 2020) (2021) 105156, http://dx.doi.org/10.1016/j.engfailanal.2020.105156.

[47] C. Farrar, G. James III, System identification from ambient vibration measurements on a bridge, J. Sound Vib. 205 (1) (1997) 1–18.

[48] O. Ditlevsen, Traffic loads on large bridges modeled as white-noise fields, J. Eng. Mech. 120 (4) (1994) 681–694.

[49] D.E. Newland, An Introduction to Random Vibrations and Spectral Analysis, Longman Publishing Group, 1984.
[50] Q. Li, Y.L. Xu, D. Wu, Concrete bridge-borne low-frequency noise simulation based on train–track–bridge dynamic interaction, J. Sound Vib. 331 (10) (2012) 2457–2470.
[51] F.D. Neeser, J.L. Massey, Proper complex random processes with applications to information theory, IEEE Trans. Inform. Theory 39 (4) (1993) 1293–1302, http://dx.doi.org/10.1109/18.243446.
[52] Y. Fujino, Y. Yoshida, Wind-induced vibration and control of Trans-Tokyo Bay crossing bridge, J. Struct. Eng. 128 (8) (2002) 1012–1025.